Phase-Shifted Full Bridge DC–DC Converter for Photovoltaic MVDC Power Collection Networks

Pierre Le Metayer, Quentin Loeuillet, Francois Wallart, Cyril Buttay, Drazen Dujic, Piotr Dworakowski

IEEE Access
Multidisciplinary ⋮ Rapid Review ⋮ Open Access Journal

Received 3 February 2023, accepted 18 February 2023, date of publication 22 February 2023, date of current version 28 February 2023.

Digital Object Identifier 10.1109/ACCESS.2023.3247952

APPLIED RESEARCH

Phase-Shifted Full Bridge DC–DC Converter for Photovoltaic MVDC Power Collection Networks

PIERRE LE MÉTAYER[1,2], QUENTIN LOEUILLET[1], FRANÇOIS WALLART[1], CYRIL BUTTAY[2], (Senior Member, IEEE), DRAZEN DUJIC[3], (Senior Member, IEEE), AND PIOTR DWORAKOWSKI[1], (Senior Member, IEEE)

[1]SuperGrid Institute, 69100 Villeurbanne, France
[2]Ampère Laboratory, Centre National de Recherche Scientifique (CNRS), Ecole Centrale de Lyon, Institut National des Sciences Appliquées (INSA) Lyon, Université Claude Bernard Lyon 1, UMR5005, 69621 Villeurbanne, France
[3]Power Electronics Laboratory, École Polytechnique Fédérale de Lausanne (EPFL), 1015 Lausanne, Switzerland

Corresponding author: Pierre Le Métayer (pierre.lemetayer@supergrid-institute.com)

This work was supported by the French National Research Agency as part of the "Investissements d'Avenir" Program under Grant ANE-ITE-002-01.

ABSTRACT The connection of photovoltaic sources to a medium voltage dc collection network requires a dc-dc converter having specific grid-connected converter capabilities. This article presents the application of a phase-shifted full bridge (PSFB) converter for medium voltage dc collection networks suited to photovoltaic power plants. The unidirectional structure of the converter is beneficial in terms of cost and simplicity of hardware implementation of the MV circuit components. The design of the PSFB converter is presented considering ratings of 250 kW power, 1.2 kV input, and 20 kV output. A converter model and a novel PSFB input voltage control regulating the dc-link voltage are developed and verified. A tuning method is given taking into account the effect of different transformer leakage inductance values. The behaviour of the PSFB under the PV power production profile and MV network faults is studied in simulation and verified against a reduced-scale prototype with ratings of 30 kW and 350 V / 600 V operating at 20 kHz. The experimental verification of the control is performed considering a real PV power profile. The experimental results under faults show the same response as in simulations. The PSFB fault response is observed to be superior compared to other dc–dc topologies with capacitive output filter only, making it suitable for grid-connected operation.

INDEX TERMS DC–DC power converters, photovoltaic systems, medium voltage.

I. INTRODUCTION

The European Commission set a 55% reduction target for greenhouse gas emissions by 2030 [1]. This ambitious target requires higher shares of renewable energy and greater energy efficiency in an integrated energy system. Just in France, based on the existing 10 GW photovoltaic (PV) installed power [2], the objective is to reach 20 GW in 2023 and 35-44 GW in 2028 [3]. This will require the development of large-scale PV power plants. PV power plants spreading over many square kilometers may benefit from electrical architectures based on medium voltage direct current (MVdc) collection networks [4], [5]. A gain in energy efficiency is expected when compared with medium voltage (MV) alternating current collection networks [6]. Moreover, the benefits of MVdc can be analyzed in terms of power dispatch, power capacity, power supply range, raw material consumption, CO_2 emissions, network resilience, and ancillary services to the ac grid. The MVdc network voltage level is expected to be around 20 kV ($\pm$10 kV), even though the optimal value depends on the power and distance [6]. Typically, the maximum voltage generated by PV strings is 1.5 kV, which is the upper limit of the low voltage (LV) range. Hence, to interface PV strings with the MVdc network, a high-ratio dc-dc converter is required.

Dc-dc converters have been well-studied for low-voltage applications. The non-isolated dc-dc converters are often derived from buck/boost topologies [7]. The isolated dc-dc

The associate editor coordinating the review of this manuscript and approving it for publication was Yuh-Shyan Hwang.

converter topologies suitable in high power applications include series resonant converters (SRC) [8] and *LLC* dc-dc resonant converters [9] (most often operated in the open loop), phase-shifted full bridge (PSFB) [10], single active bridge (SAB) [11], and dual active bridge (DAB) [12], [13] (used for bidirectional power flow). The isolated dc-dc converters involve a transformer operating at medium frequency, offering size and weight reduction [14], [15], [16] compared with an equivalent power transformer operating at 50/60 Hz.

Dc-dc converters for medium voltage applications are discussed in [17], considering three main requirements: power flow directionality, galvanic isolation, and modularity. In the case of the dc-dc converter interfacing PV strings with an MVdc network, only unidirectional power flow is required. The galvanic isolation in high-ratio dc-dc converters allows independent isolation coordination and grounding between LV and MV circuits. Moreover, an isolated dc-dc converter allows optimized power electronics design when compared to a non-isolated [18]. A monolithic converter is expected to be more cost-effective when compared to a modular one, typically because of the insulation requirements.

A unidirectional, isolated dc-dc converter was proposed in [19] for interfacing PV strings with an MVdc network. The topology is based on the isolated boost converter [20]. An inductor is added at the MVdc terminals to increase output impedance to network faults such as line short-circuit. The converter includes only one maximum power point tracking (MPPT) input, while commercial PV inverters usually present multiple inputs to achieve higher granularity for a better energy harvesting [21], [22].

In this article, a unidirectional, isolated dc-dc converter is proposed as presented in Figure 1. The system implements multiple MPPTs (each based on a boost converter), and one monolithic PSFB converter for voltage step-up and galvanic isolation. The novel contribution of this article resides in the demonstration that the well-known and simple PSFB topology is suitable for PV integration in MVdc networks, meeting the application requirements in terms of input voltage control and fault response. The control of the PSFB input dc-link voltage is derived from the ac grid-connected converters used in PV and wind applications [23], [24], [25], [26]. One of the contributions of this paper is to transpose the control scheme from ac-dc ac grid-connected converter to a dc-dc dc grid-connected converter. This paper proposes a novel and robust control scheme for the input voltage, taking into account the leakage inductance of the transformer of the PSFB converter. The control scheme regulates the LV input voltage under the PV power and MVdc voltage variations, while previous works were focused on output voltage regulation. The input impedance transfer function affected by the leakage inductance blanking time is derived in [27] but no input voltage regulation and tuning are proposed. Following the goal of the simplicity of the MV converter circuit implementation, the control relies on low-voltage circuit sensors only. Similarly, the output filter structure of the PSFB is shown to

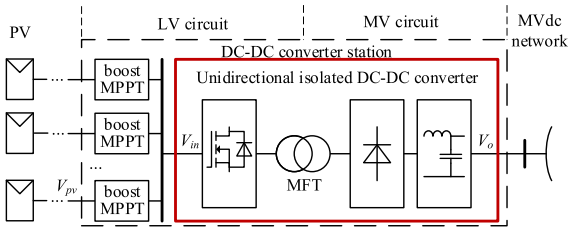

FIGURE 1. Single line diagram of the dc-dc converter station for interfacing PV with MVdc network.

be beneficial for handling faults in the MVdc network. This property is essential in network-connected converters.

This paper is organized as follows: section II presents the case study of the MVdc collection network for a PV power plant. Section III details the unidirectional isolated dc-dc converter topology and its model, and proposes a control scheme and tuning method for the input voltage regulation. Section IV gives the simulation results in transients and faults. Section V shows the experimental results based on a reduced-scale converter prototype.

II. MVDC COLLECTION NETWORK FOR PHOTOVOLTAIC POWER PLANT

A 17.3 MW PV power plant spreading linearly over 20 km is considered here [6]. This radial, ±10 kV collection network is connected on one end to the ac grid thanks to an ac-dc converter station [28] (Figure 2). The PV network voltage is 1.5 kV, corresponding to the maximum open circuit voltage of the PV, the PV voltage during production being always less than 1.2 kV. Multiple dc-dc converter stations are distributed along the collection network, each interfacing with multiple PV strings. Each dc-dc converter station includes multiple boost converters for MPPT and one isolated dc-dc converter for voltage step-up (Figure 1). Its nominal power is assumed to be 250 kW, by the power ratings of state-of-the-art PV inverters [21], [22].

A symmetric monopole line configuration with high-impedance grounding is selected for the MVdc network. It offers good robustness to fault events while reducing isolation constraints compared to the asymmetric monopole. The PV network is ungrounded, offering the possibility to still operate after a single insulation fault. Because the grounding schemes differ between PV and MVdc networks, it is required that the dc-dc converter provides a galvanic separation.

The power flow directionality is one of the major functional differences between the dc-dc converter in dc systems and the line frequency transformer in ac systems: a transformer is inherently bidirectional, but a dc-dc converter can be designed to be either unidirectional or bidirectional. In the considered MVdc collection network for the photovoltaic power plant, there is no need for the dc-dc converter to provide bidirectional power flow. Moreover, a unidirectional MVdc dc-dc converter is expected to offer a higher performance-to-cost ratio thanks to the use of diodes on the

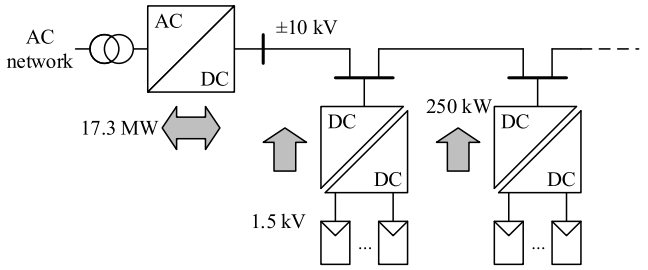

FIGURE 2. Single line diagram of the MVdc collection network for a photovoltaic power plant.

TABLE 1. Specification of the unidirectional isolated dc-dc converter.

Parameter	Value
Power flow and ratio	Unidirectional step-up
Galvanic isolation	Yes (input/output)
Modularity	No (monolithic)
Nominal Power	250 kW
Input voltage V_{in}	1.2 kV
Output voltage V_o	20 kV (±10 kV) ±10%

MV side. The use of diodes also avoids issues of power supply and control of active semiconductor devices on the MV side. The ac-dc converter in Figure 2 is assumed to be bidirectional, offering ancillary services to the ac grid (for example reactive power support).

The MVdc network voltage V_o (Figure 1) is controlled by the voltage loop of the ac-dc converter station connected to the ac grid. The control of the dc-dc converter station includes two functions. The boost MPPTs set the voltage at the PV buses V_{pv} to extract maximum power from each PV string. The isolated dc-dc converter controls its input voltage V_{in}, under power disturbances generated by MPPT converters and MVdc voltage variations.

III. UNIDIRECTIONAL ISOLATED DC–DC CONVERTER

A. TOPOLOGY

A phase-shifted full bridge (PSFB) is considered here for the isolated unidirectional dc-dc converter. This topology is composed of a low-voltage inverter, a medium frequency transformer (MFT), a medium-voltage rectifier, and an output filter comprising an inductor and a capacitor (Figure 3).

The inverter generates square waveforms, with a shift between the control signals of each leg. The PSFB is controlled by adjusting the phase shift φ between the switches in the leading leg (Q1, Q2) and those in the lagging leg (Q3, Q4). This results in the ac waveform V_P presented in Figure 4. The duty cycle D of this waveform, defined between 0 and 1, is linked to the phase shift by:

$$D = 1 - \frac{\varphi}{180°} \tag{1}$$

The PSFB components are chosen following the design rules given in [29] and [30] for a switching frequency of 20 kHz and minimum power to maintain zero voltage switching (ZVS) on both legs set at half of the nominal power. SiC

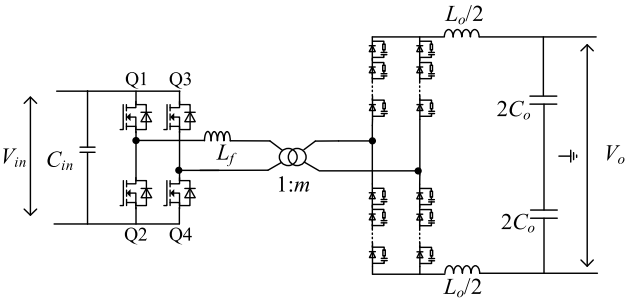

FIGURE 3. PSFB converter circuit diagram including LV inverter, medium frequency transformer, MV rectifier composed of series connected diodes with snubbers and output filter.

TABLE 2. PSFB design parameters.

Parameter/Component	Value
Switching frequency f	20 kHz
MFT turns ratio m	20.125
MFT leakage inductance L_f	5 µH
Output inductor L_o	8 mH
Input capacitor C_{in}	250 µF
Output capacitor C_o	500 pF
SiC MOSFET half-bridge modules (2 in parallel per leg)	Rohm BSM250D17P2E004
SiC Schottky diode (23 per series connection)	Genesic GD25MPS17H

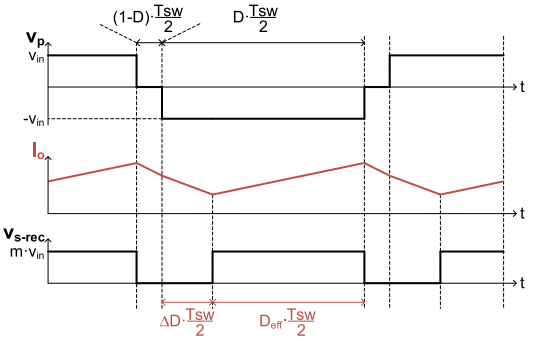

FIGURE 4. Idealized PSFB waveforms, definition of control variables (Tsw = 1/f).

MOSFET power modules are considered for the input bridge to comply with the high-efficiency requirement. Because of the low output current (12.5 A), the rectifier is considered to be made of discrete through-hole diodes. A series connection of SiC Schottky diodes of 1.7 kV voltage rating is adopted. The main design parameters are presented in Table 2. The main parameters of the magnetic components were estimated following the procedures described in [31]. Oil insulation is considered, allowing for a compact design.

B. MODEL

In a first approximation, by neglecting the leakage inductance of the transformer, a PSFB can be seen as an isolated buck converter as demonstrated in [11]. From this buck analogy, we infer the average model presented in Figure 5.

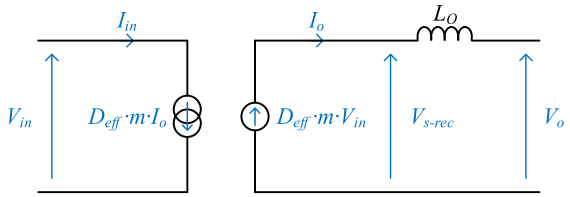

FIGURE 5. Average model of the PSFB based on buck equivalence.

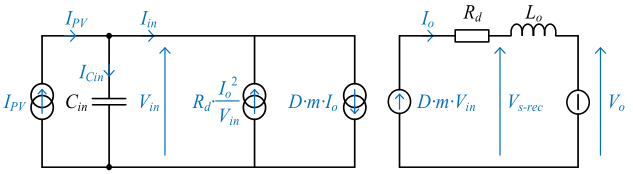

FIGURE 6. Average model of the PSFB for input voltage regulation.

However, this average model features a control variable (D_{eff}) that is not the duty cycle of the primary voltage D, and therefore cannot be controlled directly. To overcome this limitation, a series resistor is added to the dc output to represent the RMS voltage drop across the leakage inductance. Its expression is derived from the duty cycle loss expression presented in [32]:

$$\Delta D = \frac{2mL_f f}{V_{in}}\left(2I_o - \frac{V_o}{L_o}(1-D)\frac{1}{2f}\right) \tag{2}$$

where m is the turns ratio of the transformer, L_f is the leakage inductance of the transformer, f is the switching frequency, V_{in} is the input voltage, I_o is the output current, V_o is the output voltage and L_o is the output inductor. From (2), we find:

$$D = D_{eff} + \frac{4mL_f f}{V_{in}}I_o + \frac{mL_f}{V_{in}}\frac{V_o}{L_o}(D-1) \tag{3}$$

In this expression, as long as L_o is much larger than mL_f, the last term is negligible. If we define the equivalent resistance according to [33] as:

$$R_d = 4m^2 L_f f \tag{4}$$

then we get:

$$DmV_{in} \cong D_{eff}mV_{in} + R_d I_o \tag{5}$$

The conservation of power yields:

$$I_{in} = DmI_o - \frac{R_d}{V_{in}}I_o^2 \tag{6}$$

As stated previously the dc-dc converter must regulate its input voltage V_{in}. The average model including the equivalent resistance and the control variable D is represented in Figure 6.

The non-linear model is expressed as below, with g the non-linear function of states $\mathbf{x} = [I_o, V_{in}]$ and control input $u = D$, and f the function of disturbances $\mathbf{d} = [V_o, I_{PV}]$.

$$\dot{x} = \mathrm{g}(\mathbf{x}, u) + \mathrm{f}(\mathbf{d}) \tag{7}$$

$$\begin{bmatrix} \dot{I_o} \\ \dot{V_{in}} \end{bmatrix} = \begin{bmatrix} -\frac{R_d}{L_o}I_o + \frac{m}{L_o}V_{in}D \\ -\frac{m}{C_{in}}I_o D + \frac{R_d}{C_{in}}\frac{I_o^2}{V_{in}} \end{bmatrix} + \begin{bmatrix} -\frac{1}{L_o}V_o \\ \frac{1}{C_{in}}I_{PV} \end{bmatrix} \tag{8}$$

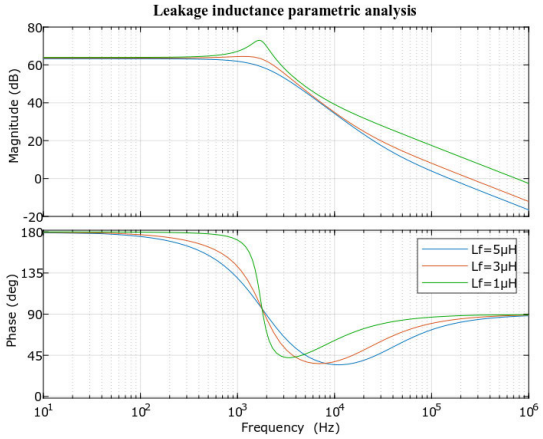

FIGURE 7. Bode diagram of PSFB transfer function H_2, with parameters from Table 2 and different values of leakage inductance $L_f = 5\ \mu$H (blue), $L_f = 3\ \mu$H (red), $L_f = 1\ \mu$H (green).

With steady-state values, for V_{inS} set to the voltage reference:

$$\dot{x_S} = f(x_S, u_S) = 0 \tag{9}$$

$$\bar{I_{oS}} = \frac{m\bar{V_{inS}}D_S - V_o}{R_d} \tag{10}$$

$$D_S = \frac{V_o^2 + I_{PV}R_d\bar{V_{inS}}}{V_o m\bar{V_{inS}}} \tag{11}$$

The linearization of the system around the operating point in steady state allows getting the transfer function $H_2(s)$ that links the input voltage to the duty cycle. This transfer function (12), as shown at the bottom of the next page, has stable poles and zeros.

A parametric analysis of the value of the leakage inductance is presented in Figure 7. One can observe the influence of the leakage inductance value on the damping of the resonance (visible for $L_f = 1\ \mu$H). Indeed, this inductance is modeled as a resistance on the dc side, damping the $C_{in}L_o$ circuit.

From equation (4) describing this resistance R_d, one can also understand that the resonance is unlikely to appear for a high conversion ratio m. Indeed, a high conversion ratio would coincide with larger leakage inductance because of the increased insulation distances, ultimately resulting in even larger R_d.

Figure 8 presents the input voltage as a function of the duty cycle for the complete range of power and output voltage. This shows that the design corresponding to the parameter values in Table 2 is compliant with the specifications from

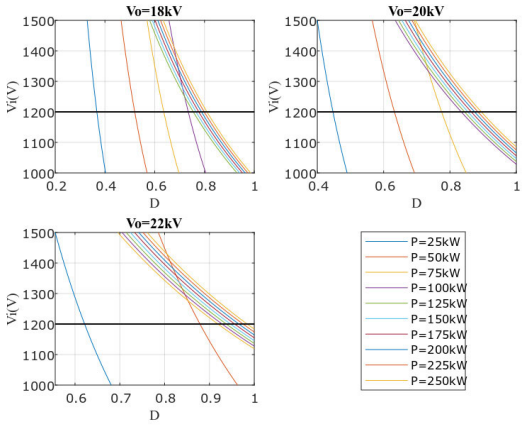

FIGURE 8. Input voltage as a function of duty cycle, for the whole range of power and the entire output voltage range.

Table 1: the input voltage can always be controlled to 1200 V with a duty cycle ranging between 0 and 1.

One can observe an important change in the duty cycle at different powers for different output voltages. This power limit corresponds to the converter entering discontinuous conduction mode, as described in [34].

C. CONTROL

The proposed control scheme is compliant with the simplicity of the unidirectional MV converter. Indeed, the only measured quantity is the low input voltage and no sensor on the MV side is necessary.

The closed-loop control system is depicted in Figure 9 with $H_2(s)$ the converter transfer function and Gc the controller transfer function. One should notice that the error signal is computed from the measured value minus the reference, as the duty cycle should be increased, extracting current from the input capacitor when the input voltage has to be decreased.

In [35] the authors propose a method to tune a Proportional Integral controller by setting the closed loop frequency at 25 times the open loop frequency. However, depending on circuit parameters and the cycle time of the controller, it is not always possible to include the resonance in the closed-loop bandwidth. If the open-loop transfer function crosses the zero gain axis around the resonance frequency shown in Figure 7, the phase margin will be too small and the control would be prone to instability.

The PI controller is defined as:

$$G_c(s) = K_p(1 + \frac{\omega_I}{s}) \tag{13}$$

with K_p the proportional part and ω_I integral part of the PI controller.

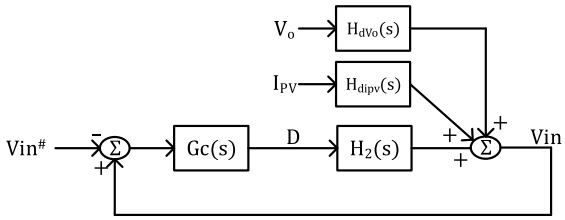

FIGURE 9. PSFB input voltage control diagram, with disturbances V_o and I_{PV}.

TABLE 3. PI controller parameters for the full-scale converter (section IV) and for the reduced-scale converter used for experimental validation (section V).

Parameter	Full scale	Reduced scale
Cut-off frequency f_c	1000 Hz	50 Hz
Proportional term K_p	3.45e-04	2.6e-04
Integral term ω_i	1.32e+04 rad/s	1669 rad/s

The proportional gain of the PI controller is obtained by keeping the maximum of the converter transfer function below −6 dB (twofold margin). K_p is therefore obtained by:

$$K_p = \frac{1/2}{\max\left(|H_2(\omega)|\right)} \tag{14}$$

The integral part of the controller takes the form of a pole at the origin and a zero at a low frequency.

$$G_I = \frac{s + \omega_I}{s} \tag{15}$$

The zero is calculated to allow the gain of the open loop transfer function to become positive at the crossover frequency ω_c:

$$\omega_I = \omega_C \sqrt{\frac{1}{\left(|H_2(\omega_c)| \cdot K_P\right)^2} - 1} \tag{16}$$

A low crossover frequency ω_c is chosen when the transfer function H_2 exhibits a resonance, so the integral part does not influence the gain at the resonant frequency. For designs not exhibiting resonance, the previous equation can still be used, with controller cycle time as the only restriction on crossover frequency.

IV. SIMULATION RESULTS

A. DYNAMIC PERFORMANCE

The PI controller on the input voltage is tuned following the method described in section III. For the design given in Table 2, the transfer function does not exhibit any resonance. Thus, the PI parameters can be calculated for a high cut-off frequency (see Table 3, full scale).

$$H_2(s) = \frac{\tilde{V_{in}}(s)}{\tilde{D}(s)} = \frac{-mV_{in_S}^2\left(mV_{in_S}D_S - R_dI_{o_S} + L_oI_{o_S} \cdot s\right)}{\left(mV_{in_S}D_S - R_dI_{o_S}\right)^2 + R_d\left(C_{in}V_{in_S}^2 + L_oI_{o_S}^2\right) \cdot \mathrm{s} + C_IL_oV_{in_S}^2 \cdot s^2} \tag{12}$$

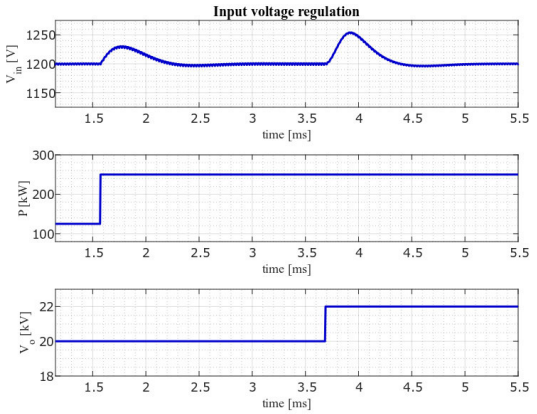

FIGURE 10. Simulation of input voltage regulation under step changes of power and output voltage.

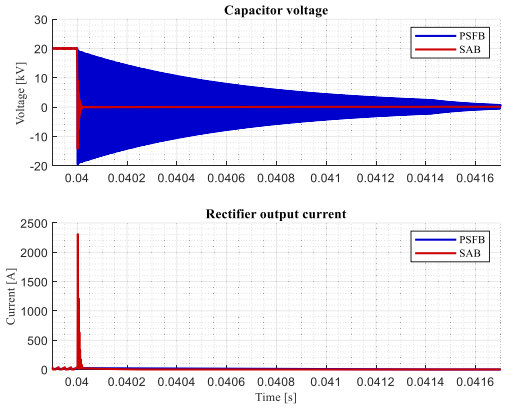

FIGURE 11. Rectifier output current during pole-to-pole fault outside converter for SAB and PSFB.

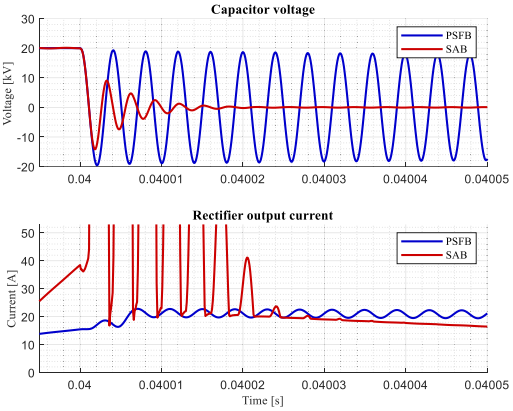

FIGURE 12. Zoom on fault instant and PSFB current.

The converter is tested with the two typical disturbances expected in operation: an input power variation (variation of I_{PV}) and an output voltage variation. The results are displayed in Figure 10. A power step from 0.5 p.u. to 1 p.u. is applied. The input voltage is regulated, with an overshoot at 1230 V (2.5%). An output voltage step from nominal to maximum (1.1 p.u.) is then applied. The input voltage is again regulated, with an overshoot at 1253 V (4.4%). One should note that such rapid step variation of power or voltage is not expected in the real application.

B. FAULT RESPONSE

The downside of having a simple passive rectifier made of diodes is that no control action can be taken on the MV side in cases of faults on the network. Once the low-voltage bridge is blocked, the only elements of the circuit affecting the fault response are the filter components. The fault response of the PSFB is studied here and compared to that of a single active bridge (SAB) [11]. The SAB is comparable to the PSFB, with the noticeable difference that it only has a capacitor across its output whereas the PSFB [17] has a capacitor and inductor. Figure 11 presents the simulated current at the output of the rectifier after a pole-to-pole fault occurring at 0.04 s at the converter terminals. The diodes of both the PSFB and the SAB are forward-biased by a negative voltage on the output capacitor due to the voltage oscillations caused by the fault current. The absence of a large inductor inside the circuit of the SAB results in very large currents capable of destroying the rectifier. For the PSFB, on the contrary, fault currents barely exceed those encountered during normal operation, as can be seen in Figure 12. It must be noted that the output inductor and capacitor interaction in the PSFB results in output voltage oscillations lasting longer than in the SAB.

V. EXPERIMENTAL VERIFICATION

A. TEST BENCH

To demonstrate the PSFB topology and control in a PV MVdc collection network, a reduced-scale system is set up. The test bench is composed of two dc-dc converters, a DAB and a PSFB in a back-to-back configuration, with a dc power supply compensating for the losses of both converters (Figure 13 and Figure 14). The test bench is controlled and monitored by a Speedgoat real-time target and programmed through Matlab Simulink Real-Time using rapid control prototyping (RCP). The converter design was detailed in [36].

In this setup, the DAB acts as the MPPT by regulating its output power, while the dc power supply represents the MVdc network and sets the PSFB output voltage. The PSFB control regulates its input voltage, ensuring the power transfer from the DAB (MPPT) to the dc power supply (MVdc network).

Figure 15 presents the implementation of the PSFB converter. Because of the low voltage output of this reduced-scale demonstration (600 V), there is no need for series-connected diodes in the rectifier bridge. As a result, the PSFB rectifier snubber is implemented using a single *RCD* snubber across the output [37] instead of multiple discrete snubbers, one for each diode. This implementation differs from the rectifier with series-connected diodes presented in section III but the experimental verification of the topology and control remains valid. Components values of the test bench converter are summarized in Table 4.

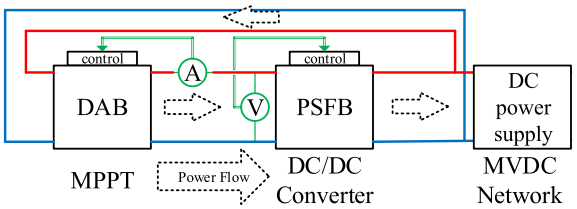

FIGURE 13. Test bench set-up block diagram including the DAB, PSFB and dc power supply, with the PV MVdc collection network equivalents (MPPT, PSFB unidirectional isolated dc-dc converter and MVdc network).

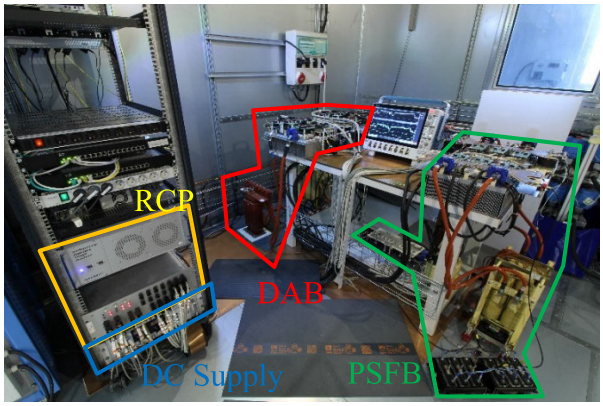

FIGURE 14. Test bench set-up.

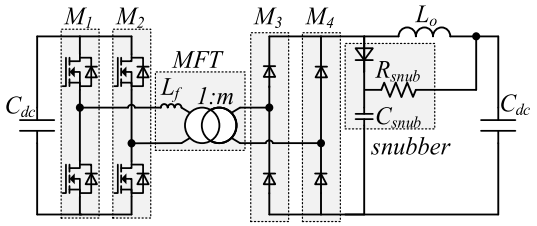

FIGURE 15. Test bench PSFB implementation, with output RCD snubber.

TABLE 4. PSFB test bench components.

Parameter/Component	Value
Input voltage V_{in}	350 V
Output voltage V_o	600 V
Operating power P	30 kW
Switching frequency f	20 kHz
Input / Output capacitor C_{dc}	160 µF
MFT turns ratio m	2
MFT leakage inductance L_f	3 µH
Switches M_x	1.7 kV, 8.0 mΩ SiC Half Bridge Module CAS300M17BM2
Snubber capacitor C_{snub}	33 nF
Snubber resistor R_{snub}	33,3 Ω
Output inductor L_o	200 µH

A second set-up is used for experiments regarding the response to faults. The PSFB input is supplied by the dc power source and its output is connected to a short-circuiting switch (Figure 16). A 1 kW load is connected to ensure proper converter operation before the short circuit instant.

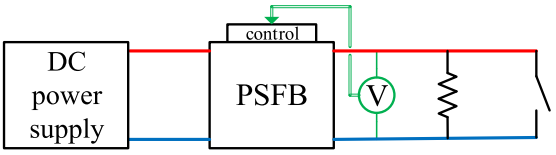

FIGURE 16. Test bench set-up for short-circuit tests.

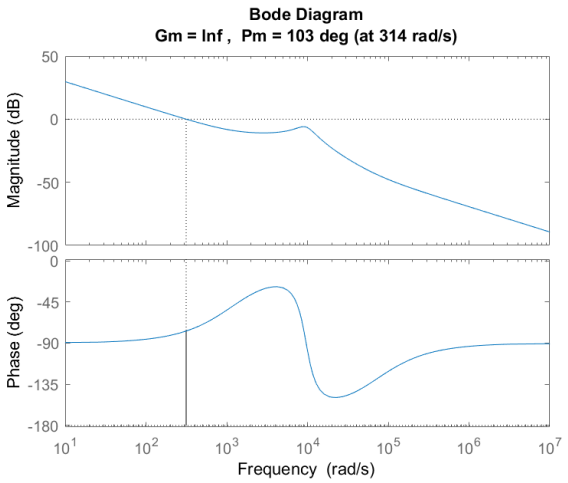

FIGURE 17. Bode diagram of open loop transfer function of controlled system for reduced scale converter tuned for a cut-off frequency of 50 Hz with gains from Table 3 (reduced scale) and parameters from Table 4, with gain margin Gm and phase margin Pm.

B. DYNAMIC PERFORMANCE

The PI regulator on the input voltage is tuned following the method described in section III for the parameters given in Table 4. For these values, the transfer function exhibits a pronounced resonance at 1520 Hz (Figure 17). Thus, a slow controller with low ω_C is chosen (cut-off frequency 50 Hz) to ensure sufficient phase-margin (see Table 3, reduced scale). It is seen in Figure 17 that the gain margin Gm is infinite in this case as the phase never reaches −180°. The phase margin Pm = 103° is largely sufficient to ensure stability. One can see that it is possible to increase the cut-off frequency to a value closer to the resonance. However, in case the real resonant frequency was lower, then the phase margin would be too low and the control would be prone to instabilities.

The control performances of the converter are evaluated in the occurrence of realistic power and output voltage variations: solar irradiance measurements are taken from [38] and scaled to the test bench power. The high sampling rate of these data (up to 1 ms) enables a good reproduction of real PV dynamics. This power profile is reproduced by the DAB converter which regulates the power in the back-to-back configuration and mimics the MPPT in the target application. The dc supply voltage is also changed arbitrarily throughout the test. This represents voltage variations in the MVdc network. Experimental results are shown in Figure 18.

One should note that this experimental validation is considered the worst case in terms of control compared to the full-scale system. Indeed, the presence of a non-damped resonance in the system results in the tuning of the controller with

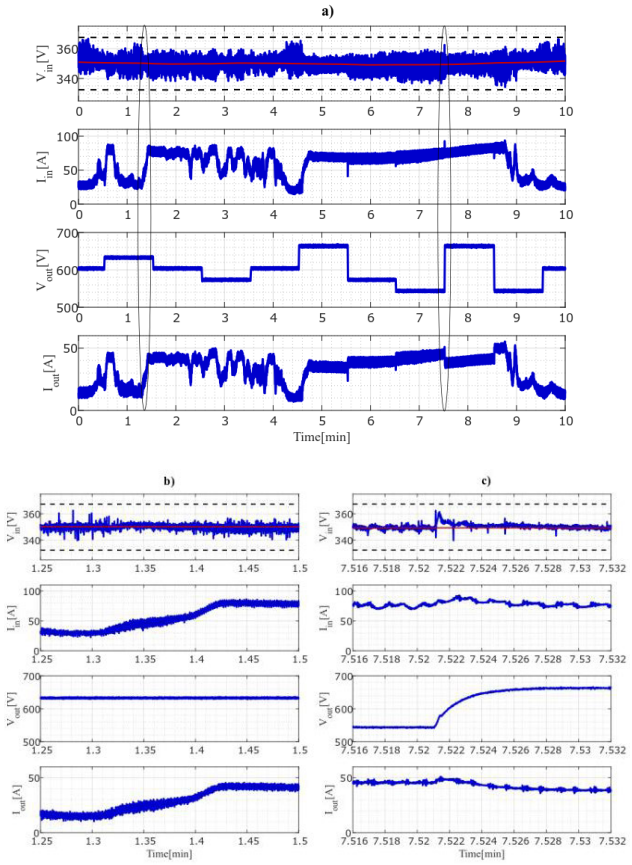

FIGURE 18. Experimental waveforms: a) Input voltage V_{in} regulated to 350 V, input current I_{in} following the PV profile for maximum power of 30 kW, output voltage V_{out} = 600 V with step variations in the range ±10 % of output voltage, output current I_{out}. b) Zoom on input current change from 30 A to 80 A. c) Zoom on output voltage change from 540 V to 660 V.

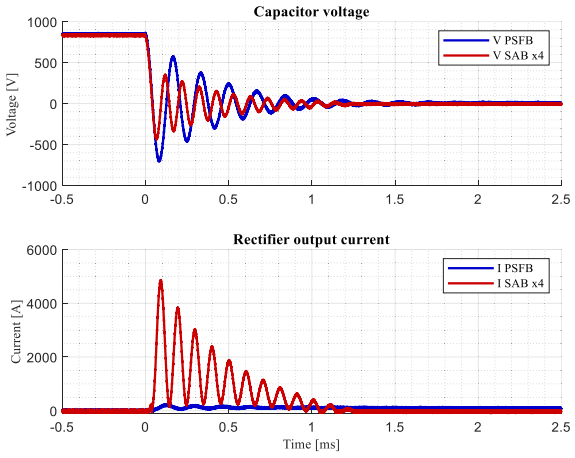

FIGURE 19. Experimental waveforms of output capacitor voltage and rectifier output current of PSFB (blue) and SAB (red) after an output short-circuit at 800 V.

a low cut-off frequency, which translates to a slow response of the controller. Yet, it is observed that the input voltage is regulated to the target value of 350 V during the whole test with a maximum deviation of 5% when faced with an output voltage variation of ±10% at 400 V/s together with an input power varying from 6 to 30 kW with a time dynamic which replicates a day with a very variable irradiance. The regulation of the input voltage under these variations of input power and output voltage shows the reliability of the control for a wide variety of operating points.

C. RESPONSE TO FAULT

The fault response of the PSFB and SAB converters is tested by creating a low resistance (20 mΩ) short-circuit at output terminals as shown in Figure 16. Experimental results are presented in Figure 19.

The output voltage is controlled at 800 V for the PSFB and 200 V for the SAB before closing the short-circuiting switch. The primary bridge is stopped shorty (≈50μs) after the fault is declared for the primary bridge not to contribute to the short-circuit current. The test voltage of the SAB was reduced to 200 V to avoid any damage to the rectifier bridge. In Figure 19 the voltage and current of the SAB are scaled to 800 V.

Experimental results show the same phenomenon as presented in section IV-B. The peak value of the SAB rectifier output current is 4.8 kA for an output voltage of 800 V. The current decreases back to 0 A in 1.2 ms. Designing the rectifier for withstanding such an event would result in the use of largely overrated diodes.

VI. CONCLUSION

A unidirectional, isolated, dc-dc converter is analyzed in the scope of an MVdc collection network for photovoltaic power plants. The converter topology is based on the arrangement of multiple boost converters for maximum power point tracking and one phase-shifted full bridge converter for voltage step-up and galvanic isolation. The unidirectional structure is considered beneficial in terms of cost and simplicity of implementation. A design of the PSFB converter is realized at 250 kW and 1.2 kV / 20 kV, to fulfill the requirements of the target application. A PSFB converter model is developed and a control scheme is proposed to regulate the LV input voltage required by the application. The LV input voltage control is realized by taking into account the effect of the transformer leakage inductance and with inputs only from LV side sensors. The PSFB exhibits low fault currents without any active control, a very interesting feature compared with converters having a purely capacitive output filter. A reduced scale prototype (30 kW power, 350 V / 600 V input/output voltage, and a 20 kHz switching frequency) is developed to validate the PSFB converter topology and control. It is tested under a real PV power profile, demonstrating the ability of the converter to meet the operational requirements of the MVdc collection network. The experimental results fit well the simulations, proving the accuracy of the proposed design and modeling. The fault behavior of PSFB and SAB converters are validated in the experiment, showing the benefits of the output inductor for the protection of the diode bridge in case of an MVdc network fault.

REFERENCES

[1] European Commission. *The European Commission'S Priorities*. Accessed: Jul. 26, 202. [Online]. Available: https://ec.europa.eu/info/strategy/priorities-2019-2024_en

[2] D. Salel and F. Delpit, "Etat du photovoltaïque en France," Ademe, Angers, France, 2019.

[3] Ministere de la Transition Ecologique. *Programmations Pluriannuelles De L'Energie (PPE)*. Accessed: Jul. 26, 2021. [Online]. Available: https://www.ecologie.gouv.fr/programmations-pluriannuelles-lenergie-ppe

[4] A. Cabrera-Tobar, E. Bullich-Massagué, M. Aragüés-Peñalba, and O. Gomis-Bellmunt, "Topologies for large scale photovoltaic power plants," *Renew. Sustain. Energy Rev.*, vol. 59, pp. 309–319, Jun. 2016.

[5] H. A. B. Siddique, S. M. Ali, and R. W. De Doncker, "DC collector grid configurations for large photovoltaic parks," in *Proc. 15th Eur. Conf. Power Electron. Appl. (EPE)*, Sep. 2013, pp. 1–10.

[6] P. Le Metayer, J. Paez, S. Toure, C. Buttay, D. Dujic, E. Lamard, and P. Dworakowski, "Break-even distance for MVDC electricity networks according to power loss criteria," in *Proc. 23rd Eur. Conf. Power Electron. Appl. (EPE ECCE Europe)*, Sep. 2021, pp. 1–9.

[7] K. Tytelmaier, O. Husev, O. Veligorskyi, and R. Yershov, "A review of non-isolated bidirectional DC–DC converters for energy storage systems," in *Proc. Int. Young Scientists Forum Appl. Phys. Eng. (YSF)*, Oct. 2016, pp. 22–28.

[8] F. C. Schwarz and J. B. Klaassens, "A controllable 45-kW current source for DC machines," *IEEE Trans. Ind. Appl.*, vol. IA-15, no. 4, pp. 437–444, Jul. 1979.

[9] J. Zhang, W. Jiang, T. Jiang, S. Shao, Y. Sun, B. Hu, and J. Zhang, "A three-port LLC resonant DC/DC converter," *IEEE J. Emerg. Sel. Topics Power Electron.*, vol. 7, no. 4, pp. 2513–2524, Dec. 2019.

[10] L. H. Mweene, C. A. Wright, and M. F. Schlecht, "A 1 kW 500 kHz front-end converter for a distributed power supply system," *IEEE Trans. Power Electron.*, vol. 6, no. 3, pp. 398–407, Jul. 1991.

[11] K. Park and Z. Chen, "Analysis and design of a parallel-connected single active bridge DC–DC converter for high-power wind farm applications," in *Proc. 15th Eur. Conf. Power Electron. Appl. (EPE)*, Sep. 2013, pp. 1–10.

[12] J. Xue, F. Wang, D. Boroyevich, and Z. Shen, "Single-phase vs. three-phase high density power transformers," in *Proc. IEEE Energy Convers. Congr. Expo.*, Sep. 2010, pp. 4368–4375.

[13] R. W. A. A. De Doncker, D. M. Divan, and M. H. Kheraluwala, "A three-phase soft-switched high-power-density DC/DC converter for high-power applications," *IEEE Trans. Ind. Appl.*, vol. 27, no. 1, pp. 63–73, Jan. 1991.

[14] M. Mogorovic and D. Dujic, "100 kW, 10 kHz medium-frequency transformer design optimization and experimental verification," *IEEE Trans. Power Electron.*, vol. 34, no. 2, pp. 1696–1708, Feb. 2019.

[15] I. Villar, L. Mir, I. Etxeberria-Otadui, J. Colmenero, X. Agirre, and T. Nieva, "Optimal design and experimental validation of a medium-frequency 400 kVA power transformer for railway traction applications," in *Proc. IEEE Energy Convers. Congr. Expo. (ECCE)*, Sep. 2012, pp. 684–690.

[16] G. Ortiz, J. Biela, D. Bortis, and J. W. Kolar, "1 megawatt, 20 kHz, isolated, bidirectional 12 kV to 1.2 kV DC–DC converter for renewable energy applications," in *Proc. Int. Power Electron. Conf.*, Jun. 2010, pp. 3212–3219.

[17] P. Dworakowski, P. Le Metayer, C. Buttay, and D. Dujic, "Unidirectional step-up isolated DC–DC converter for MVDC electrical networks," *Presented at CIGRE Session*, 2022.

[18] J. D. Paez, J. Maneiro, S. Bacha, D. Frey, and P. Dworakowski, "Influence of the operating frequency on DC–DC converters for HVDC grids," in *Proc. 21st Eur. Conf. Power Electron. Appl. (EPE ECCE Europe)*, Sep. 2019, p. 10.

[19] H. Wang, Y. Zhou, X. Huang, Y. Wang, and H. Xu, "Topology and control strategy of PV MVDC grid-connected converter with LVRT capability," *Appl. Sci.*, vol. 11, no. 6, p. 2739, Mar. 2021.

[20] E.-S. Park, S. J. Choi, J. M. Lee, and B. H. Cho, "A soft-switching active-clamp scheme for isolated full-bridge boost converter," in *Proc. 19th Annu. IEEE Appl. Power Electron. Conf. Expo.*, Feb. 2004, pp. 1067–1070.

[21] *ABB String Inverters PVS-175-TL*, ABB, Datasheet, Dec. 2018. [Online]. Available: https://www.bath.ac.uk/publications/library-guides-to-citing-referencing/attachments/ieee-style-guide.pdf

[22] *SG250HX Multi-MPPT String Inverter for 1500 Vdc System*, Sungrow, Datasheet, 2019. [Online]. Available: https://www.bath.ac.uk/publications/library-guides-to-citing-referencing/attachments/ieee-style-guide.pdf

[23] J. M. S. Callegari, A. F. Cupertino, V. D. N. Ferreira, and H. A. Pereira, "Minimum DC-link voltage control for efficiency and reliability improvement in PV inverters," *IEEE Trans. Power Electron.*, vol. 36, no. 5, pp. 5512–5520, May 2021.

[24] L. Huang, C. Wu, D. Zhou, and F. Blaabjerg, "Comparison of DC-link voltage control schemes on grid-side and machine-side for type-4 wind generation system under weak grid," in *Proc. 47th Annu. Conf. IEEE Ind. Electron. Soc.*, Oct. 2021, pp. 1–6.

[25] S. F. Zarei, H. Mokhtari, M. A. Ghasemi, S. Peyghami, P. Davari, and F. Blaabjerg, "DC-link loop bandwidth selection strategy for grid-connected inverters considering power quality requirements," *Int. J. Electr. Power Energy Syst.*, vol. 119, Jul. 2020, Art. no. 105879.

[26] D. Zouheyr, B. Lotfi, L. Thierry, and B. Abdelmadjid, "Grid side inverter control for a grid connected synchronous generator based wind turbine experimental emulator," *Eur. J. Electr. Eng.*, vol. 23, no. 1, pp. 1–7, Feb. 2021.

[27] D. Ochoa, A. Lázaro, P. Zumel, M. Sanz, J. R. De Frutos, and A. Barrado, "Small-signal modeling of phase-shifted full-bridge converter considering the delay associated to the leakage inductance," *Energies*, vol. 14, no. 21, p. 7280, Nov. 2021.

[28] A. Khonya, "AC-DC converters for medium voltage direct current networks with integrated renewable energy sources," M.S. thesis, Dept. Energy, Politecnico di Milano, 2021.

[29] G. Liu, K. Wang, C. Qu, S. Liu, Q. Jia, and Y. Li, "Phase-shift full bridge power supply based on SiC devices," *J. Eng.*, vol. 2018, no. 13, pp. 453–460, Jan. 2018.

[30] R. Ullah, A. Ali, and Z. Ullah, "Zero voltage switched full bridge converters for the battery charger of electric vehicle," *Int. J. Energy Power Eng.*, vol. 10, no. 9, pp. 1183–1192, Jul. 2016.

[31] A. Fouineau, M. Guillet, B. Lefebvre, M.-A. Raulet, and F. Sixdenier, "A medium frequency transformer design tool with methodologies adapted to various structures," in *Proc. 15th Int. Conf. Ecol. Vehicles Renew. Energies (EVER)*, 2020, pp. 1–14.

[32] V. Vlatkovic, J. A. Sabate, R. B. Ridley, F. C. Lee, and B. H. Cho, "Small-signal analysis of the phase-shifted PWM converter," *IEEE Trans. Power Electron.*, vol. 7, no. 1, pp. 128–135, Jan. 1992.

[33] G. D. Capua, S. A. Shirsavar, M. A. Hallworth, and N. Femia, "An enhanced model for small-signal analysis of the phase-shifted full-bridge converter," *IEEE Trans. Power Electron.*, vol. 30, no. 3, pp. 1567–1576, Mar. 2015.

[34] M. J. Schutten and D. A. Torrey, "Improved small-signal analysis for the phase-shifted PWM power converter," *IEEE Trans. Power Electron.*, vol. 18, no. 2, pp. 659–669, Mar. 2003.

[35] M. Villalva and E. Filho, "Buck converter with variable input voltage for photovoltaic applications," in *Proc. 9th Brazilian Power Electron. Conf.*, Blumenau, Brazil, 2007, pp. 1–6.

[36] T. Lagier et al., "How good are the design tools in power electronics?" in *Proc. 22nd Eur. Conf. Power Electron. Appl. (EPE ECCE Europe)*, 2020, pp. P.1–P.12.

[37] I. Ferencz, D. Petreus, and T. Patarau, "Comparative study of three snubber circuits for a phase-shift converter," in *Proc. Int. Symp. Power Electron., Electr. Drives, Autom. Motion (SPEEDAM)*, Jun. 2020, pp. 763–768.

[38] Natural Resources Canada. (Apr. 25, 2016). *High-Resolution Solar Radiation Datasets*. Accessed: Jul. 26, 2021. [Online]. Available: https://www.nrcan.gc.ca/energy/renewable-electricity/solar-photovoltaic/18409

PIERRE LE MÉTAYER received the B.Sc. and M.Sc. degrees in electrical engineering from the Institut National des Sciences Appliquées (INSA) Lyon, Lyon, in 2019, where he is currently pursuing the Ph.D. degree in power electronics. He is working with the SuperGrid Institute and the Ampère Laboratory. His research interests include dc–dc converters, medium voltage systems, and integration of renewable energy sources.

QUENTIN LOEUILLET received the B.Sc. and M.Sc. degrees in electrical engineering from the Grenoble Institute of Technology, in 2017 and 2020, respectively. He is currently pursuing the Ph.D. degree in industrial engineering with Valeo and G2ELAB, on the optimal design of electric powertrain systems. In 2020, he joined the SuperGrid Institute as a Research Engineer.

FRANÇOIS WALLART received the M.Sc. degree in electrical engineering from the Hautes Etudes Industrielles, Lille, France, in 1998.

From 2000 to 2008, he worked with Alstom Transport, Tarbes, France, on traction drives control and then with Alstom Transport, Villeurbanne, France, on permanent magnet synchronous motor control. Since 2015, he has been in charge of control of power converters at the SuperGrid Institute, Villeurbanne. He has coauthored more than ten scientific publications and four patent applications. His research interest includes power electronic converters and systems for electric drives.

CYRIL BUTTAY (Senior Member, IEEE) received the engineering and Ph.D. degrees from the Institut National des Sciences Appliquées (INSA) Lyon, Lyon, France, in 2001 and 2004, respectively.

From 2005 to 2007, he was a Research Associate with the Electrical Machines and Drives Research Team, University of Sheffield, Sheffield, U.K., and with the Power Electronics Machines and Control Group, University of Nottingham, Nottingham, U.K. Since 2008, he has been a Scientist with the French Centre National de Recherche Scientifique (CNRS), and has worked with Ampère Laboratory, Lyon, on the topic of packaging for power electronics, with a special focus on high-temperature, high-voltage, or high-density applications. From 2019 to 2020, he was a Visiting Scholar with the Center for Power Electronics Systems (CPES), Virginia Tech, Blacksburg, VA, USA. Since 2021, he has been the Deputy Director of the Ampère Laboratory.

DRAZEN DUJIC (Senior Member, IEEE) received the Dipl.-Ing. and M.Sc. degrees in electrical engineering from the University of Novi Sad, Novi Sad, Serbia, in 2002 and 2005, respectively, and the Ph.D. degree in electrical engineering from Liverpool John Moores University, Liverpool, U.K., in 2008.

From 2002 to 2006, he was a Research Assistant with the Department of Electrical Engineering, University of Novi Sad. From 2006 to 2009, he was a Research Associate with Liverpool John Moores University. From 2009 to 2013, he was with ABB Corporate Research Center, Switzerland, as a Principal Scientist, working on power electronics projects spanning the range from low-voltage/power SMPS in below kilowatt range to medium voltage high-power converters in a megawatt range. From 2010 to 2011, he was a member of a project team responsible for the development of the world's first power electronic traction transformer which was successfully commissioned on a locomotive. From 2013 to 2014, he was with ABB Medium Voltage Drives, Turgi, Switzerland, as a Research and Development Platform Manager, responsible for ABB's largest IGCT-based medium-voltage drive ACS6000. He is currently with the École Polytechnique Fédéralen de Lausanne (EPFL), Lausanne, Switzerland, as an Associate Professor and the Director of the Power Electronics Laboratory. He has authored or coauthored more than 200 scientific publications and has filed 20 patents. His current research interest includes the design and control of advanced high-power electronics systems for medium-voltage applications.

Dr. Dujic received the First Prize Paper Award from the Electric Machines Committee of the IEEE Industrial Electronics Society, in 2007. In 2014, he received the Isao Takahashi Power Electronics Award for outstanding achievement in power electronics. In 2018, he received the EPE Outstanding Service Award from the European Power Electronics and Drives Association. He is an Associate Editor of IEEE TRANSACTIONS ON POWER ELECTRONICS.

PIOTR DWORAKOWSKI (Senior Member, IEEE) received the M.Sc. and Ph.D. degrees in electrical engineering from the Gdańsk University of Technology, Poland, in 2007 and 2020, respectively.

From 2008 to 2013, he was a Research and Development Engineer with Alstom, Tarbes, France. Since 2014, he has been a Research and Development Manager with the SuperGrid Institute, Lyon, France. He is the author of more than 50 scientific articles and two CIGRE technical brochures related to HVDC and MVDC. He is also the inventor of several patent applications. His research interest includes power electronics converters and systems for renewable energy integration.

Dr. Dworakowski is a member of the CIGRE French National Committee and the International Scientific Committee of the European Power Electronics and Drives Association. He has actively contributed to several working groups. His Ph.D. dissertation on medium-frequency transformers received the distinction from the Scientific Council of Control, Electronic and Electrical Engineering at the Gdańsk University of Technology and two awards: one from the French Chapter of the IEEE Power and Energy Society, in 2020, and the second in the contest organized by the Warsaw University of Technology and Siemens, in 2021.